

# Majorana fermion fingerprints in spin-polarised scanning tunneling microscopy

Panagiotis Kotetes<sup>1,\*</sup>, Daniel Mendler<sup>1,2</sup>, Andreas Heimes<sup>1</sup>, and Gerd Schön<sup>1,2</sup>

<sup>1</sup>*Institut für Theoretische Festkörperphysik, Karlsruhe Institute of Technology, 76131 Karlsruhe, Germany and*

<sup>2</sup>*Institute of Nanotechnology, Karlsruhe Institute of Technology, 76344 Eggenstein-Leopoldshafen, Germany*

We calculate the spatially resolved tunneling conductance of topological superconductors (TSCs) based on ferromagnetic chains, measured by means of spin-polarised scanning tunneling microscopy (SPSTM). Our analysis reveals novel signatures of MFs arising from the interplay of their *strongly anisotropic* spin-polarisation and the magnetisation content of the tip. We focus on the deep Yu-Shiba-Rusinov (YSR) limit where only YSR bound states localised in the vicinity of the adatoms govern the low-energy as also the topological properties of the system. Under these conditions, we investigate the occurrence of zero/finite bias peaks (ZBPs/FBPs) for a single or two coupled TSC chains forming a Josephson junction. Each TSC can host up to two Majorana fermions (MFs) per edge if chiral symmetry is preserved. Here we retrieve the conductance for all the accessible configurations of the MF number of each chain. Our results illustrate innovative spin-polarisation-sensitive experimental routes for arresting the MFs by either restoring or splitting the ZBP in a predictable fashion via: i) weakly breaking chiral symmetry, e.g. by the SPSTM tip itself or by an external Zeeman field and ii) tuning the superconducting phase difference of the TSCs, which is encoded in the  $4\pi$ -Josephson coupling of neighbouring MFs.

## I. INTRODUCTION

Recent experiments in hybrid superconducting devices [1–3] have revealed strong evidence for the existence of Majorana fermions (MFs) [4–6], which are neutral non-abelian zero-energy quasiparticle excitations in many-particle systems. The unambiguous confirmation of their discovery and their successful experimental manipulation will be an evidence for this exotic kind of statistics and in addition will constitute fertile ground for developing topological quantum computing [7]. The first experiments claiming the discovery of MFs have been performed in platforms based on semiconducting nanowires [1] with strong spin-orbit coupling (SOC), a type of artificial topological superconductors (TSCs) predicted in Ref. 8. One of the most distinctive features of an isolated MF is the appearance of a zero bias peak (ZBP) of height  $2e^2/h$  in the tunneling conductance [9, 10]. However, a ZBP is not unique to MFs [11] and thus a number of experiments [12] have scrutinised the findings concerning the possible presence of MFs in such devices.

The particular debate opened the door to new ideas for engineering MFs without involving semiconductors but by instead employing devices based on conventional SCs in the presence of some kind of magnetic texture. One of the first proposals along this direction [13] pinpointed that a magnetic chain with randomly ordered spins deposited onto a SC can harbor MFs at its edges. Later on it was realised [14, 15] that in the absence of SOC and other external fields the presence of a helical magnetic texture is the minimal requirement for engineering a TSC [6]. More importantly, TSCs from magnetic chains on superconducting substrates can be manipulated and probed using spin-polarised scanning tunneling microscopy (SPSTM) [16], allowing the spatial visualisation of the MF

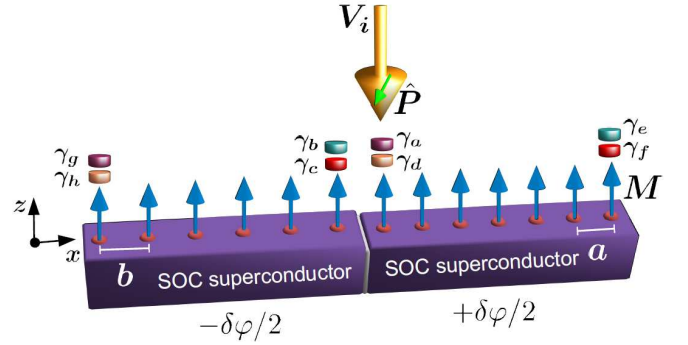


FIG. 1. Two coupled topological superconductors (TSCs) based on magnetic chains probed by means of spin-polarised scanning tunneling microscopy (SPSTM). The tip electrons owe a spin-polarisation along the  $\hat{P}$  direction. Each chain can host 1 or 2 MFs per edge by virtue of chiral symmetry. The two TSCs are interfaced by a thin insulator yielding a Josephson junction since the superconducting phases on the two chains differ by  $\delta\varphi$ . By tuning the orientation of  $\hat{P}$ , the value of  $\delta\varphi$ , as also by controllably violating or restoring chiral symmetry, one can imprint Majorana fermion (MF) signatures on the tunneling conductance  $dI_i/dV_i$ .

wavefunctions and thus providing a more reliable method for diagnosing TSCs. This advantage further motivated a plethora of theoretical proposals involving helical magnetism [17]. Remarkably, it has been also shown that helicity (or SOC) can be artificially engineered using suitable external fields for the case of antiferromagnetically ordered chains [18]. If instead SOC is present, both ferromagnetic [19–26] and antiferromagnetic [21, 22] chains on a SC can exhibit topologically non-trivial properties and host MFs. As a matter of fact, the first situation appears to have been recently realised [2]. Nonetheless, further experiments at lower temperatures and with im-

\* panagiotis.kotetes@kit.edu

proved energy resolution are required for confirming the presence of MFs [2, 25].

In this work we illustrate a number of yet unexplored experimental fingerprints of MFs which can be directly tested in the existing devices [2], thus promising an unambiguous identification of the MFs. Key feature of our approach is properly taking into account the magnetic spin-polarisation content of the SPSTM tip, which can also provide a natural explanation for the very low value of the measured conductance in the above mentioned experiment. Previous studies have focused on a non-magnetic tip in the normal [23, 25] or superconducting phase [27]. Following the method of Ref. 10 we retrieve the tunneling conductance for ferromagnetically ordered chains within the microscopic Yu-Shiba-Rusinov (YSR) [28–31] model, extracted in Ref. 21. The latter electronic bound states dominate the low-energy properties of the substrate SC in the presence of the magnetic adatoms. If the atomic spins can be treated as classical, the YSR states become fully responsible for the topological properties of the hybrid device. As it has been shown in Ref. 21 such topological YSR bands can harbor 1 or 2 MFs per edge in the presence of chiral symmetry.

Specifically, we investigate the tunneling conductance properties and the emerging zero/finite bias peaks (ZBPs/FBPs) for i) isolated chains supporting either number of MFs per edge and ii) pairs of coupled chains with the same or different number of MFs per edge. Central feature of our analysis is the electronic spin-polarisation induced by the MFs, which exhibits a strongly anisotropic coupling to the tip electrons, transferring this distinctive behaviour to the tunneling conductance. Evenmore, depending on the spin-polarisation of the magnetic tip, chiral symmetry can be weakly violated locally in a controlled manner. The latter can drastically affect the conductance spectra and the qualitative features of the ZBPs. In the case of the coupled chains we additionally consider a finite phase difference in the order parameters of the SCs, yielding  $4\pi$ -periodic Josephson MF couplings [32], which can further control the location of the peaks. This collection of fingerprints appear feasible to be looked for in existing platforms [2] and capable of unveiling the presence of MFs.

## II. THEORETICAL MODEL AND METHODS

In the following section we present in detail our theoretical approach and model. In Sec. IIA we review the topological properties and model of a single ferromagnetic YSR chain. The form of the related MF wavefunctions and the inter-MF coupling in the case of two tunnel-coupled TSCs are both discussed in Sec. IIB. The SPSTM tip Hamiltonian and its coupling to the MFs is contained in Secs. IIC and IID. Finally, the steps for the calculation of the tunneling conductance by employing the Keldysh formalism are explained in Sec. IIE.

### A. Topological ferromagnetic YSR chain

In a previous work, Ref. 21, three of the present authors extracted the microscopic topological model describing the YSR bands of a ferromagnetic chain deposited on a superconducting substrate with Rashba SOC. The YSR bands arise from the overlap of YSR bound states which lie energetically deep below the energy scale set by the bulk superconducting gap. For extracting this low energy model, one starts from the Hamiltonian of the bulk SC with Rashba SOC

$$H_{\text{SC}} = \frac{1}{2} \sum_{\mathbf{k}} \Psi_{\mathbf{k}}^{\dagger} [\xi_{\mathbf{k}} \tau_z + \alpha \tau_z (\mathbf{k} \times \hat{z}) \cdot \tilde{\sigma} - \Delta \tau_y \sigma_y] \Psi_{\mathbf{k}}, \quad (1)$$

where the Pauli matrices  $\sigma$  and  $\tau$  are defined in spin and particle-hole space respectively,  $\tilde{\sigma} = (\tau_z \sigma_x, \sigma_y, \tau_z \sigma_z)$ , while  $\Psi_{\mathbf{k}}^{\dagger} = (\psi_{\mathbf{k}\uparrow}^{\dagger}, \psi_{\mathbf{k}\downarrow}^{\dagger}, \psi_{-\mathbf{k}\uparrow}, \psi_{-\mathbf{k}\downarrow})$  is the corresponding spinor. The operators  $\psi_{\mathbf{k},\sigma}^{\dagger}$  create electrons of momentum  $\mathbf{k}$  and spin-projection  $\sigma$ . Here  $\xi_{\mathbf{k}}$  corresponds to the free electron energy dispersion,  $\alpha$  denotes the SOC strength and  $\Delta$  the bulk superconducting gap. Straightforward manipulations allow us to obtain a Hamiltonian describing the electrons of the SC, localised at the adatom sites. The corresponding Schrödinger equation in site space  $i, j$  has the form (see Ref. 21)

$$\sum_j \hat{H}_{ij} \phi_j = \varepsilon \phi_i \quad (2)$$

with  $\phi_i^{\dagger} = (u_{i,\uparrow}^*, u_{i,\downarrow}^*, v_{i,\uparrow}, v_{i,\downarrow})$  and the Hamiltonian

$$\hat{H}_{ij} = \frac{\Delta}{\pi \nu_F M^2} \left[ (\pi \nu_F M^2 \tau_y \sigma_y - M \tau_z \sigma_z) \delta_{ij} + M^2 (G_{i-j}^s \tau_z - G_{i-j}^a \tau_z \sigma_y + F_{i-j}^s \tau_y \sigma_y - F_{i-j}^a \tau_y) \right], \quad (3)$$

with the Fermi-level density of states (DOS) in the normal phase of the SC,  $\nu_F$ .  $M = JS$  denotes the ferromagnetic energy scale, with  $J$  the exchange energy between the SC electrons and the adatoms with spin  $S$ . The solution of Eq. (2) determines the energies and wavefunctions of the YSR midgap states, with the coefficients

$$\frac{G^s(r)}{\pi \nu_F} = \cos(k_F \alpha r / v_F) \sin(k_F |r| - \frac{\pi}{4}) e^{-\frac{|r|}{\xi_0}} \sqrt{\frac{2}{\pi k_F |r|}}, \quad (4)$$

$$\frac{F^s(r)}{\pi \nu_F} = \cos(k_F \alpha r / v_F) \cos(k_F |r| - \frac{\pi}{4}) e^{-\frac{|r|}{\xi_0}} \sqrt{\frac{2}{\pi k_F |r|}}, \quad (5)$$

$$\frac{G^a(r)}{i \pi \nu_F} = \sin(k_F \alpha r / v_F) \sin(k_F |r| - \frac{\pi}{4}) e^{-\frac{|r|}{\xi_0}} \sqrt{\frac{2}{\pi k_F |r|}}, \quad (6)$$

$$\frac{F^a(r)}{i \pi \nu_F} = \sin(k_F \alpha r / v_F) \cos(k_F |r| - \frac{\pi}{4}) e^{-\frac{|r|}{\xi_0}} \sqrt{\frac{2}{\pi k_F |r|}}, \quad (7)$$

where  $\xi_0$  is the coherence length of the SC,  $k_F$  ( $v_F$ ) the Fermi wave-vector (velocity) and  $r = (i - j)a$  with the adatom spacing  $a$ . Note that  $G^{a,s}(0) = F^{a,s}(0) = 0$ . The indices  $s$  and  $a$  denote functions which are symmetric or

anti-symmetric under inversion  $r \rightarrow -r$ . In the rest of the manuscript we use  $k_F$  in units of  $\pi/a$ ,  $\alpha$  in units of  $v_F$ ,  $M$  in units of  $1/(\pi v_F)$  and  $\xi_0$  in units of  $a$ .

By transferring to  $k$ -space we obtain the Bogoliubov-de Gennes (BdG) Hamiltonian

$$\hat{\mathcal{H}}_k = t_k \tau_z - v_k \tau_z \sigma_y + (\Delta + \mathcal{D}_k) \tau_y \sigma_y - d_k \tau_y - \mathcal{B} \tau_z \sigma_z, \quad (8)$$

where we have introduced  $\mathcal{B} = \Delta/(\pi v_F J S)$  and

$$t_k = \sum_{\delta=1}^{\infty} t_{\delta} \cos(\delta k a) \quad \text{with} \quad t_{\delta} = \frac{2\Delta}{\pi v_F} G_{\delta}^s, \quad (9)$$

$$v_k = \sum_{\delta=1}^{\infty} v_{\delta} \sin(\delta k a) \quad \text{with} \quad v_{\delta} = \frac{2\Delta}{i\pi v_F} G_{\delta}^a, \quad (10)$$

$$\mathcal{D}_k = \sum_{\delta=1}^{\infty} \mathcal{D}_{\delta} \cos(\delta k a) \quad \text{with} \quad \mathcal{D}_{\delta} = \frac{2\Delta}{\pi v_F} F_{\delta}^s, \quad (11)$$

$$d_k = \sum_{\delta=1}^{\infty} d_{\delta} \sin(\delta k a) \quad \text{with} \quad d_{\delta} = \frac{2\Delta}{i\pi v_F} F_{\delta}^a. \quad (12)$$

The BdG Hamiltonian above resides in symmetry class BDI [6, 21], with time-reversal symmetry  $\Theta = \mathcal{K}$  ( $\Theta^2 = I$ ), chiral symmetry  $\Pi = \tau_x$  and charge-conjugation  $\Xi = \tau_x \mathcal{K}$ , where  $\mathcal{K}$  denotes complex conjugation. The particular symmetry class supports a  $\mathbb{Z}$  topological invariant [33] allowing an integer number of MFs per chain edge. The detailed diagram of 0, 1 and 2 MF phases per edge has been extracted in Ref. 21 as also in others works within different frameworks [20, 34]. Topological YSR chains with multiple MFs edge modes can be found also in two-dimensional systems [35].

External perturbations which violate chiral symmetry  $\Pi$  (or equivalently  $\Theta$ ) enforce the system to reside in symmetry class D, which allows up to a single MF per edge. This implies that if the TSC resides in the topological phase with 2 MFs per edge, the application of an *infinitesimally weak*  $\Pi$ -violating perturbation  $m$ , will unavoidably hybridise the 2 MFs, splitting them into finite energy (proportional to  $m$ ) bound states. However, the 1 MF per edge phase remains unaffected by such a weak field. Symmetry analysis demonstrates that the simplest source of chiral symmetry breaking is a Zeeman field applied along the  $y$  axis, i.e.  $B_y$ . Instead  $B_x$  and  $B_z$  fields preserve the latter. The  $B_y$  field can be either applied globally or only near the edge, since it will always hybridise the 2 MFs sitting at the same edge. Notably in a SPSTM experiment the tip itself is magnetised, and depending on its magnetic orientation can controllably violate or preserve  $\Pi$ . The latter property has significant ramifications when measuring the tunneling conductance with the SPSTM technique, and can influence the possible observation of the ZBP or its quantisation with a single or double unit of conductance ( $2e^2/h$ ).

## B. Majorana wavefunctions and their coupling

By solving Eq. (3) for a finite chain, one can retrieve the MF wavefunctions which have the special form

$$\Phi_{i,n}^{\dagger} = (u_{i,\uparrow,n}^*, u_{i,\downarrow,n}^*, u_{i,\uparrow,n}, u_{i,\downarrow,n}), \quad (13)$$

with the wavefunction components satisfying  $\sum_{i,\sigma} |u_{i,\sigma,n}|^2 = 1/2$ . The latter normalisation implies the anticommutation relation for the corresponding MF operators  $\{\gamma_n, \gamma_m\} = \delta_{n,m}$ . For a low energy description, one can focus only on the MF sector and neglect the rest of the BdG quasiparticles which lie above the bulk superconducting gap. Thus in the low energy limit, we can approximate the YSR state operators with the MF operators, i.e.,  $\psi_{i,\sigma} = \sum_n u_{i,\sigma,n} \gamma_n$ . In the presence of suitable symmetries and ideal conditions (e.g. infinite chains) the MFs operators remain unpaired [4], while in any realistic situation one has to introduce also couplings for the MFs, yielding the following general coupled MF Hamiltonian

$$\mathcal{H}_{\text{MF}} = \frac{i}{2} \sum_{n,m} \mathcal{M}_{nm} \gamma_n \gamma_m. \quad (14)$$

Solely residing on the above MF description is a good approximation only as long as the coupling elements  $\mathcal{M}_{nm}$  are much smaller compared to the YSR bandstructure gap. As long as this is case, the matrix elements can arise due to the following reasons: i) a weak chiral symmetry breaking term, e.g.  $m$ , coupling for instance 2 MFs at the same edge previously protected by  $\Pi$ , ii) finite size of the chains which can allow the overlap of MFs primarily located at the far edges, giving rise to quasiparticles with finite energy splitting  $\delta\epsilon$  and iii) coupling  $M$  of neighbouring MFs located at the edge of two different tunnel-coupled TSC chains. For the purposes of our discussion MF coupling matrix elements of the first type will be discussed at a phenomenological level, while for the others we will explicitly calculate the couplings by employing the BdG formalism and considering a particular model for inter-chain tunneling, respectively.

For inferring the coupling of edge MFs due to the inter-chain tunneling, we focus on the electronic degrees of the two substrate SCs and consider that they are separated by a thin insulating film yielding a Josephson junction with a corresponding superconducting phase difference  $\delta\varphi$ . The latter can be imposed by inducing a supercurrent flow through the junction or by gluing together the very left and right edges of a single chain in order to form a ring through which we can thread flux. To this end, we assume that the electrons of the two substrate SCs are coupled via the Hamiltonian

$$\mathcal{H}_T = \sum_{i,j} \left[ \psi_{i,\sigma}^{\dagger} T_{i,j} e^{i(\varphi_i - \varphi_j)/2} \psi_{j,\sigma} + \text{H.c.} \right]. \quad (15)$$

In particular, here we consider the profile

$$T_{i,j} = t \frac{1 - \text{sgn}(i \cdot j)}{2} \exp \left[ -\frac{|ai - bj| - (a + b)}{l} \right]. \quad (16)$$

In the above we have already assumed that one TSC chain resides on the positive sites  $i, j > 0$  and the other on the negative ones. In this manner, the projector  $[1 - \text{sgn}(i \cdot j)]/2$  allows only interchain tunneling, while we have also assumed that the tunneling strength decays exponentially with the distance  $|ia - jb|$  over a characteristic decay length  $l$ , with  $a, b$  denoting the adatom spacings of each chain. Moreover, in the above Hamiltonian we have incorporated the spatially varying superconducting phase profile  $\varphi_i$ , which here is assumed to have the form  $\varphi_i = \text{sgn}(i)\delta\varphi/2$ . The corresponding MF matrix elements that one obtains take the following form

$$M_{nm} = 4 \text{Im} \sum_{i,j,\sigma} u_{i,\sigma,n}^* T_{i,j} e^{i(\varphi_i - \varphi_j)/2} u_{j,\sigma,m}. \quad (17)$$

### C. SPSTM tip Hamiltonian

For the purposes of this work we model the SPSTM tip at site  $i$ , as a lead of spinful electrons under the influence of a spin splitting field  $\mathbf{P}$ . Moreover, here we assume that the tip feels a voltage  $V_i$ , which is responsible for driving the coupled system out of equilibrium and leads to the tunneling current. Previous works on the tunneling conductance for such systems have considered a non-magnetic tip in the normal [23, 25] or the superconducting phase [27]. The tip Hamiltonian has the form

$$\mathcal{H}_{\text{TIP},i} = \sum_{\mathbf{k},\alpha,\beta} [(\epsilon_{\mathbf{k}} - eV_i)\delta_{\alpha\beta} - \mathbf{P} \cdot \boldsymbol{\sigma}_{\alpha\beta}] c_{\mathbf{k},\alpha,i}^\dagger c_{\mathbf{k},\beta,i}. \quad (18)$$

Here by keeping the index  $i$  for the tip electrons and the voltage we allow our formalism to address the case of a multi-tip SPSTM, while in the most general case we should include an index  $i$  also to the spin-polarisation  $\mathbf{P}$ . The latter can be parametrised in the following way

$$\mathbf{P} = P(\cos \vartheta \sin \eta, \sin \vartheta \sin \eta, \cos \eta). \quad (19)$$

The presence of  $\mathbf{P}$  modifies the DOS for the spin up and down electrons  $\rho_\sigma(E)$  at energy  $E$ . In particular the normalised DOS read

$$\nu_\sigma = \rho_\sigma(E)/\rho(E) \quad \text{with} \quad \rho(E) = \sum_\sigma \rho_\sigma(E), \quad (20)$$

where  $\rho_\uparrow - \rho_\downarrow \propto P$ . At this point we perform a rotation and diagonalise the tip Hamiltonian in spin space using the property

$$\mathbf{P} \cdot \boldsymbol{\sigma} = \hat{R}^\dagger P \sigma_z \hat{R}, \quad \hat{R} = \exp(i\eta\sigma_y/2) \exp(i\vartheta\sigma_z/2). \quad (21)$$

Thus the tip Hamiltonian becomes

$$\mathcal{H}_{\text{TIP},i} = \sum_{\mathbf{k},\sigma=\pm} (\epsilon_{\mathbf{k},\sigma} - eV_i) \tilde{c}_{\mathbf{k},\sigma,i}^\dagger \tilde{c}_{\mathbf{k},\sigma,i}. \quad (22)$$

with  $\sigma = \pm$  labelling the two eigenstates of  $\sigma_z$  with eigenvalues  $\pm 1$  and  $\epsilon_{\mathbf{k},\sigma} = \epsilon_{\mathbf{k}} - \sigma P$ .

### D. Coupling between the SPSTM tip and the MFs

The SPSTM tip originally couples to the electronic density of the superconducting substrate at site  $i$ , via the tunneling Hamiltonian

$$\mathcal{H}_{\text{TIP-MF},i} = \sum_{\mathbf{k},\sigma} \left( T_{\mathbf{k},i} c_{\mathbf{k},\sigma,i}^\dagger \psi_{i,\sigma} + \text{H.c.} \right). \quad (23)$$

After diagonalising the tip Hamiltonian in spin space we obtain

$$\mathcal{H}_{\text{TIP-MF},i} = \sum_{\mathbf{k},\sigma,n} \left( \mathcal{V}_{\mathbf{k},\sigma,i,n} \tilde{c}_{\mathbf{k},\sigma,i}^\dagger - \mathcal{V}_{\mathbf{k},\sigma,i,n}^* \tilde{c}_{\mathbf{k},\sigma,i} \right) \gamma_n, \quad (24)$$

with the matrix elements

$$\mathcal{V}_{\mathbf{k},\sigma,i,n} = \sum_{\sigma'} T_{\mathbf{k},i} R_{\sigma,\sigma'} u_{i,\sigma',n}. \quad (25)$$

### E. Tunneling conductance

After having set the stage for calculating the tunneling conductance, we can proceed with deriving the Heisenberg operator for the current through the tip located over site  $i$

$$\begin{aligned} \hat{I}_i(t) &= -e \dot{N}_{\text{TIP}}(t) = -e \sum_{\mathbf{k},\sigma} \frac{d}{dt} \left( \tilde{c}_{\mathbf{k},\sigma,i}^\dagger(t) \tilde{c}_{\mathbf{k},\sigma,i}(t) \right) \\ &= -\frac{e\hbar}{\hbar} \sum_{\mathbf{k},\sigma} \left[ \mathcal{H}_{\text{TIP-MF},i}, \tilde{c}_{\mathbf{k},\sigma,i}^\dagger \tilde{c}_{\mathbf{k},\sigma,i} \right] (t). \end{aligned} \quad (26)$$

The current operator in the Schrödinger picture reads

$$\hat{I}_i = \frac{e\hbar}{\hbar} \sum_{\mathbf{k},\sigma,n} \left( \mathcal{V}_{\mathbf{k},\sigma,i,n} \tilde{c}_{\mathbf{k},\sigma,i}^\dagger + \mathcal{V}_{\mathbf{k},\sigma,i,n}^* \tilde{c}_{\mathbf{k},\sigma,i} \right) \gamma_n. \quad (27)$$

The expectation value of the current operator  $I_i(t) \equiv \langle \hat{I}_i(t) \rangle$  is calculated from the expression

$$\begin{aligned} I_i(t) &= \frac{2e}{\hbar} \sum_{\mathbf{k},\sigma,n} \text{Im} \left[ \mathcal{V}_{\mathbf{k},\sigma,i,n}^* \langle \gamma_n(t) \tilde{c}_{\mathbf{k},\sigma,i}(t) \rangle \right] \\ &= -\frac{2e}{\hbar} \sum_{\mathbf{k},\sigma,n} \text{Re} \left[ \mathcal{V}_{\mathbf{k},\sigma,i,n}^* G_{\mathbf{k},\sigma,i,n}^<(t,t) \right], \end{aligned} \quad (28)$$

which involves the lesser mixed Green's function

$$G_{\mathbf{k},\sigma,i,n}^<(t,t') \equiv i \langle \gamma_n(t') \tilde{c}_{\mathbf{k},\sigma,i}(t) \rangle. \quad (29)$$

For calculating the current one can employ the Keldysh formalism and introduce the respective Keldysh-contour-ordered Green's functions. After following this route we find that for retrieving the final expression for the current we will need the retarded MF Green's functions

$$\mathcal{G}_{nm}^R(t,t') \equiv -i\Theta(t-t') \langle \gamma_n(t) \gamma_m(t') \rangle. \quad (30)$$

Since here we are interested in the non-equilibrium steady state, one can follow the method of Ref. 10 and show that

the expectation value of the current operator is given by the formula

$$I_i = \frac{e}{h} \int_{-\infty}^{+\infty} d\omega \mathcal{T}_i(\omega) [n_F(\omega - eV_i) - n_F(-\omega + eV_i)], \quad (31)$$

with the Fermi-Dirac distribution  $n_F(\omega)$  at energy  $\omega$  and the transmission coefficient

$$\mathcal{T}_i(\omega) \equiv \text{Tr} \left[ \hat{\mathcal{G}}^R(\omega) \hat{\Gamma}^{i*}(-\omega) \hat{\mathcal{G}}^A(\omega) \hat{\Gamma}^i(\omega) \right], \quad (32)$$

according to terminology of the Landauer-Büttiker formalism. Note however that in contrast to the usual Landauer formula for ballistic transport in normal conductors, the present formula involves one electron and one hole Fermi-Dirac distribution. This is a direct consequence of the involvement of MFs which are equal superpositions of electrons and holes. The matrix elements for the linewidth hermitian matrices  $\hat{\Gamma}^i(\omega)$  are given by the expression

$$\Gamma_{nm}^i(\omega) = 2\pi \sum_{\mathbf{k}, \sigma} \mathcal{V}_{\mathbf{k}, \sigma, i, n}^* \mathcal{V}_{\mathbf{k}, \sigma, i, m} \delta(\omega - \epsilon_{\mathbf{k}, \sigma}). \quad (33)$$

As in Ref. 10 we adopt the wideband approximation according to which the linewidth matrix elements can be considered to be energy independent. In particular, we assume that  $\mathbf{T}_{\mathbf{k}, i} = \mathbf{T}$  (the  $\mathbf{k}$  independence reflects the wideband approximation) and set the DOS of the tip to be approximately  $\rho_\sigma(E_F)$ . The latter consideration yields

$$\Gamma_{nm}^i(\omega) \equiv \Gamma_{nm}^i = \Gamma \mathbf{u}_{i, n}^\dagger \frac{\mathbb{1} + P_s \hat{\mathbf{P}} \cdot \boldsymbol{\sigma}}{2} \mathbf{u}_{i, m}, \quad (34)$$

with  $\Gamma = 2\pi\rho(E_F)|\mathbf{T}|^2$ ,  $\mathbf{u}_{i, n}^\dagger = (u_{i, \uparrow, n}^*, u_{i, \downarrow, n}^*)$  and the unit vector  $\hat{\mathbf{P}} = \mathbf{P}/P$ . Furthermore we introduced the spin polarisation degree  $P_s = \nu_\uparrow - \nu_\downarrow$  ( $\sum_\sigma \nu_\sigma = 1$ ). Note that for convenience we set  $\Gamma = 1$ , a convention which we will follow throughout the remainder of the manuscript. For retrieving the transmission coefficient one has to calculate the retarded and advanced MF matrix Green's functions given by

$$\hat{\mathcal{G}}^R(\omega) = \left( \omega \hat{I} - i\hat{\mathcal{M}} + i \text{Re} \hat{\Gamma}^i \right)^{-1}, \quad (35)$$

where  $\hat{\mathcal{G}}^A(\omega) = [\hat{\mathcal{G}}^R(\omega)]^\dagger$ . In the above we have considered that the self-energies of the MF matrix Green's functions contain only the linewidth functions, in the spirit of the wideband approximation as in Ref. 10.

For the rest of our discussion, we will focus on the *zero temperature* tunneling conductance given by the following expression

$$\frac{dI_i}{dV_i} = \frac{2e^2}{h} \mathcal{T}_i(eV). \quad (36)$$

### III. RESULTS AND DISCUSSION

In the following paragraphs we present our results concerning the tunneling conductance for a single or two coupled TSC magnetic chains. In particular the case of a single chain is examined in Secs. III A and III B where we analyse TSCs with 1 and 2 MFs per edge, respectively. Later on, we consider the situation of two coupled TSC chains with the superconducting phases of the substrate SCs differing by  $\delta\varphi$ , thus allowing a  $4\pi$ -periodic Josephson coupling between the neighbouring edge MFs. In particular, in Sec. III C we consider two chains, each of which harbors a single MF per edge. In Sec. III D(III E) we investigate Josephson junctions consisting of a TSC chain with a single MF per edge and a TSC chain with 2 MFs per edge, where we assume that the SPSTM tip couples to the chain hosting 1(2) MFs per edge. In Sec. III F we considered a Josephson junction of two TSC chains each of which hosts 2 MFs per edge. In the whole discussion particular emphasis will be given to chiral symmetry violation and restoration, and its implications for observing the ZBPs which are considered smoking gun signatures of MFs.

#### A. One TSC chain with 1 MF per edge

In the present paragraph we discuss the case of an isolated chain with a single MF per edge as shown in Fig. 2. Similarly to the result of Ref. 10 the tunneling conductance in this case takes the simple Lorentzian form

$$\frac{dI_i}{dV} = \frac{2e^2}{h} \frac{(\Gamma_{aa}^i)^2}{(eV)^2 + (\Gamma_{aa}^i)^2}, \quad (37)$$

from which one recovers the ZBP with one quantum of conductance. In the above and from now on, we set  $V_i \equiv V$  for convenience. The broadening is given by the expression

$$\Gamma_{aa}^i = \Gamma \mathbf{u}_{i, a}^\dagger \frac{\mathbb{1} + P_s \hat{\mathbf{P}} \cdot \boldsymbol{\sigma}}{2} \mathbf{u}_{i, a}. \quad (38)$$

Crucial feature of our analysis is the inclusion of the magnetic characteristics of the SPSTM tip which opens new perspectives for detecting MFs. In fact, one observes that if  $\hat{\mathbf{P}} \cdot \boldsymbol{\sigma} \mathbf{u}_{i, a} = -\mathbf{u}_{i, a}$  the linewidth term becomes  $\Gamma_{aa}^i = \nu_\downarrow \Gamma \mathbf{u}_{i, a}^\dagger \mathbf{u}_{i, a}$ . If the tip becomes fully spin polarised, so that  $\nu_\downarrow = 0$ , the tunneling conductance will also go to zero and the ZBP will disappear from the tunneling spectra. Essentially, when these conditions are met, the spin polarisation of the tip-electrons is antiparallel to the electronic edge polarisation  $\langle \boldsymbol{\sigma} \rangle_i = \mathbf{u}_{i, a}^\dagger \boldsymbol{\sigma} \mathbf{u}_{i, a}$  induced by the MF. Therefore the tip-MF coupling becomes zero since tunneling between the tip and the substrate electrons is spin conserving and cannot take place for antiparallel polarisations.

As shown in Fig. 3 the MFs of both sides of a single chain induce an electronic spin-polarisation which is

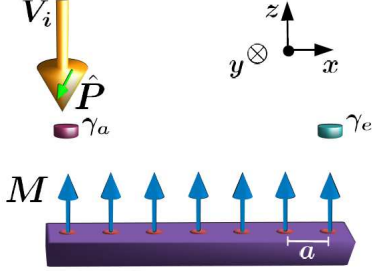


FIG. 2. TSC based on a ferromagnetically ordered atomic chain probed by SPSTM. The tip is considered to couple locally, i.e. only to the electronic density directly below it. For long chains only the  $\gamma_a$  MF is seen by the probe, while for short ones both MFs contribute.

confined in the  $x - z$  plane, as a result of the complex conjugation symmetry  $\Theta = \mathcal{K}$  which forces the spin-part of the wavefunction to be real. The particular distinctive feature, allows us to employ a SPSTM tip for unveiling the MFs. In particular, one obtains a characteristic anisotropic dependence of the tunneling conductance on the angles  $(\vartheta, \eta)$  which determine the tip-magnetisation.

In order to make a connection to the realistic situation, potentially relevant to the experiment of Ref. 2, we further take into account the influence of the remaining MF away from the tip. If the overlap of the MF wavefunctions is non-negligible due to the short length of the chain, a finite coupling of the form  $\nu\delta\epsilon\gamma_a\gamma_e$  will appear leading to finite energy excitations. More importantly, for short chains the tip generally couples to both MFs. In this case we have

$$\widehat{\mathcal{M}} = \begin{pmatrix} 0 & \delta\epsilon \\ -\delta\epsilon & 0 \end{pmatrix} \quad \text{and} \quad \widehat{\Gamma}^i = \begin{pmatrix} \Gamma_{aa}^i & \Gamma_{ae}^i \\ (\Gamma_{ae}^i)^* & \Gamma_{ee}^i \end{pmatrix}, \quad (39)$$

yielding the modified tunneling conductance formula

$$\begin{aligned} \frac{dI_i}{dV} &= \frac{2e^2}{h} \left\{ 2 \left[ \det(\text{Re} \widehat{\Gamma}^i) + \delta\epsilon^2 \right] \det \widehat{\Gamma}^i \right. \\ &\quad \left. + (eV)^2 \left[ (\Gamma_{aa}^i)^2 + (\Gamma_{ee}^i)^2 + 2(\text{Re}^2 \Gamma_{ae}^i - \text{Im}^2 \Gamma_{ae}^i) \right] \right\} \cdot \\ &\quad \left\{ \left[ (eV)^2 - \delta\epsilon^2 - \det(\text{Re} \widehat{\Gamma}^i) \right]^2 + (eV)^2 (\Gamma_{aa}^i + \Gamma_{ee}^i)^2 \right\}^{-1}, \end{aligned} \quad (40)$$

For  $V = 0$  one obtains the simple result

$$\left. \frac{dI_i}{dV} \right|_{V=0} = 2 \cdot \frac{2e^2}{h} \frac{\Gamma_{aa}^i \Gamma_{ee}^i - |\Gamma_{ae}^i|^2}{\Gamma_{aa}^i \Gamma_{ee}^i - \text{Re}^2 \Gamma_{ae}^i + \delta\epsilon^2}, \quad (41)$$

which provides the ZBP height in this general case. Strikingly, when both MFs are accessed by the tip, the ZBP *persists*, though with a conductance with reduced spectral weight from the ideal value. This ZBP appears due the coupling of the tip to the  $\gamma_e$  MF, and directly disappears if we set  $\Gamma_{ee}^i = \Gamma_{ae}^i = 0$ . Apart from the residual spectral weight for  $V = 0$ , the conductance shows finite bias peaks

$$eV = \pm \sqrt{\delta\epsilon^2 + \det(\text{Re} \widehat{\Gamma}^i)}, \quad (42)$$

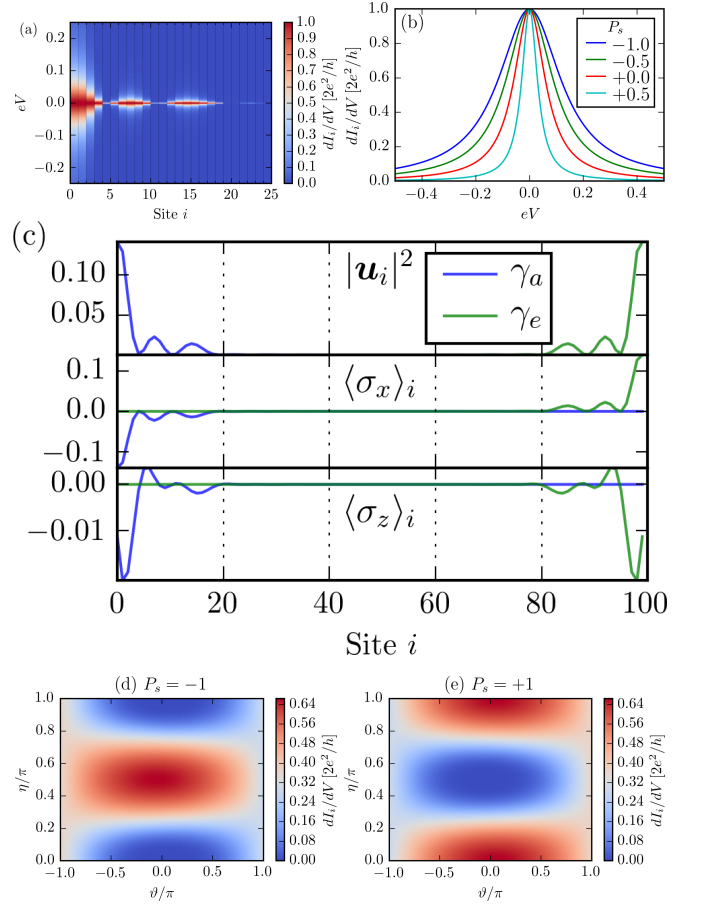


FIG. 3. SPSTM tip coupled to a single MF for the case of a sufficiently long chain of  $N = 100$  sites. (a) Spatial profile of the tunneling conductance for a spin unpolarised tip ( $P_s = 0$ ). (b) Spatial profile of the tunneling conductance profile for a tip polarised along the  $x$  axis for varying  $P_s$ . The modification of the polarisation degree alters the profile broadening. (c) Local spectral weight ( $|u_i|^2$ ) and electronic spin polarisation ( $\langle \sigma \rangle$ ) of the two MFs. Note that the spin polarisation along the  $y$  axis is exactly *zero* as a result of  $\Theta = \mathcal{K}$  symmetry. (d, e) Tunneling conductance as a function of the angles  $(\vartheta, \eta)$  for the case of a fully polarised tip  $P_s = \pm 1$ . The present maps show the strong electronic spin anisotropy induced by the MF  $\gamma_a$  and constitutes one of its characteristic signatures. Parameters:  $\xi_0 = 80$ ,  $k_F = 6.0$ ,  $\alpha = 0.01$  and  $M = 0.85$ .

as shown in Fig. 5. The tunneling conductance for these voltages reads

$$\left. \frac{dI_i}{dV} \right|_{\text{FBPs}} = \frac{2e^2}{h} \frac{(\Gamma_{aa}^i + \Gamma_{ee}^i)^2 - 4 \text{Im}^2 \Gamma_{ae}^i}{(\Gamma_{aa}^i + \Gamma_{ee}^i)^2}. \quad (43)$$

Notably the FBPs have a height equal to  $2e^2/h$  only if  $\text{Im} \Gamma_{ae}^i = 0$ . Otherwise, the height is lower. As inferred by Fig. 4, the quantised case is in good approximation for all the cases except when probing with a magnetic tip with polarisation along the  $z$  axis. In this case, the tunneling conductance is *much weaker*. As a matter of fact, this is exactly the configuration employed in the experi-



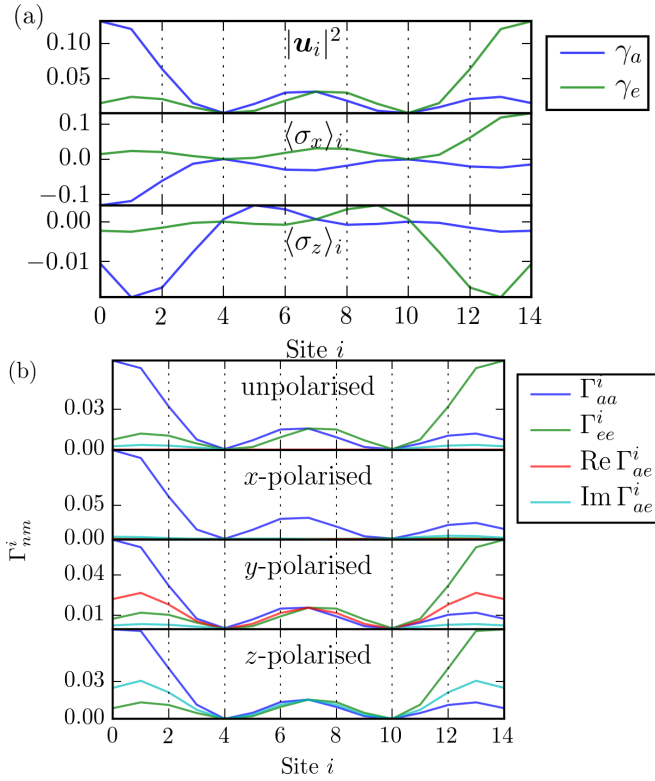


FIG. 4. (a) Spectral weight of MF wavefunctions and their induced electronic spin-polarisation in the case of a short chain consisting of  $N = 15$  sites. The two MFs hybridise and form finite energy quasiparticle excitations. (b) Matrix elements of the linewidth matrix  $\hat{\Gamma}^i$ . For each case of tip full spin-polarisation, we present only the non-zero elements. Parameters:  $\xi_0 = 80$ ,  $k_F = 6.0$ ,  $\alpha = 0.01$  and  $M = 0.85$ .

ment of Ref. 2 and our findings can provide one possible explanation to the highly reduced signal, aside from the unavoidable temperature broadening. According to our theory, orienting the spin-polarisation of the tip along the  $x, y$  axes will drastically increase the conductance value to almost a single quantum, while we additionally obtain that the ZBP can be found even for very short chains of  $N = 15$  sites. These remarkable findings are depicted in more detail in Fig. (5) and demonstrate once again that SPSTM is a powerful tool for detecting these MF fingerprints attributed to the anisotropic MF spin-polarisation.

Finally, if the coupling of the tip to  $\gamma_e$  is completely negligible, then the tunneling conductance formula reads (see also Ref. 10)

$$\frac{dI_i}{dV} = \frac{2e^2}{h} \frac{(eV)^2 (\Gamma_{aa}^i)^2}{[(eV)^2 - \delta\epsilon^2]^2 + (eV)^2 (\Gamma_{aa}^i)^2}. \quad (44)$$

From the above expression we see that the ZBP *disappears* and splits into two FBP appearing for  $eV = \pm\delta\epsilon$ .

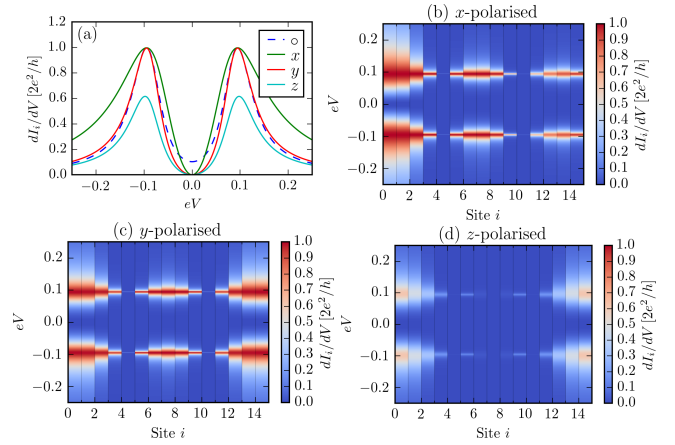


FIG. 5. Spatial tunneling conductance profile in the case of a short chain consisting of  $N = 15$  sites. (a) Profile at site  $i = 1$  for spin unpolarised ( $\circ$ ) and fully polarised tip along the  $x, y, z$  axes. For a spin unpolarised tip one finds residual spectral weight for  $V = 0$ . Due to the spin anisotropy in the MF induced spin-polarisation we observe a significant difference in the height of the FBPs. When the polarisation is confined in the  $x - y$  plane or the tip is unpolarised, the conductance is practically equal to  $2e^2/h$ , while for a tip magnetised along the  $z$  axis one obtain a reduced height. We present the complete spatial profile for a fully spin-polarised tip along the  $x, y, z$  axis in (b-d). Note the spectral weight asymmetry in b). Parameters:  $\xi_0 = 80$ ,  $k_F = 6.0$ ,  $\alpha = 0.01$  and  $M = 0.85$ .

## B. One TSC chain with 2 MFs per edge

In this paragraph we examine the case of a single TSC magnetic chain where due to the preservation of chiral symmetry 2 MFs appear per edge as in Fig. 6. For simplicity we assume that the two edges are infinitely separated allowing us to restrict ourselves to the MF subspace of  $\gamma_a$  and  $\gamma_d$ . Essentially we exclude coupling between MFs of different edges and at the same time assume negligible coupling between the tip electrons and the MFs located at the right edge. Consequently, both MFs on the left edge couple to the tip, while they can also couple to each other with a matrix element  $m$ , arising due to weakly broken chiral symmetry. As we have already underlined the latter violation can be a consequence of the SPSTM tip itself, if the polarisation contains a component along the  $y$  axis. Under these conditions we have

$$\hat{\mathcal{M}} = \begin{pmatrix} 0 & m \\ -m & 0 \end{pmatrix} \quad \text{and} \quad \hat{\Gamma}^i = \begin{pmatrix} \Gamma_{aa}^i & \Gamma_{ad}^i \\ (\Gamma_{ad}^i)^* & \Gamma_{dd}^i \end{pmatrix}, \quad (45)$$

which are identical to the ones found in Eq. (39) with the correspondence  $m \rightarrow \delta\epsilon$  and  $d \rightarrow e$ . Note that here the off-diagonal elements for the linewidth functions are crucial and cannot be neglected a priori, since the two chiral symmetry protected MFs have spectral weight at the same region. This is in stark contrast to Sec. III A as also previous studies [10] where the overlap of the 2 MFs involved can be completely neglected in the infinite sepa-

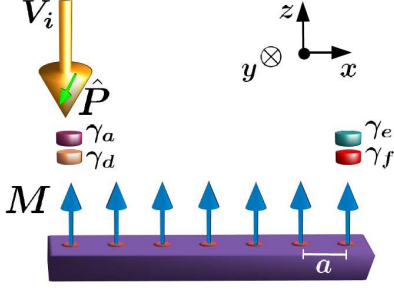


FIG. 6. TSC harboring 2 MFs per edge protected by chiral symmetry. For sufficiently long chains the two MFs below the SPSTM probe tip need to be taken into account for inferring the tunneling spectra. When owing a polarisation component along the  $y$  axis, the magnetic tip itself can break locally chiral symmetry and hybridise the two MFs, even in the absence of other symmetry breaking fields.

ration limit. The tunneling conductance can be obtained from Eq. (41) after performing the replacement  $\delta\epsilon \rightarrow m$  and  $e \rightarrow d$ . For  $V = 0$  one obtains

$$\frac{dI_i}{dV}\bigg|_{V=0} = 2 \cdot \frac{2e^2}{h} \frac{\Gamma_{aa}^i \Gamma_{dd}^i - |\Gamma_{ad}^i|^2}{\Gamma_{aa}^i \Gamma_{dd}^i - \text{Re}^2 \Gamma_{ad}^i + m^2}. \quad (46)$$

As previously, the ZBP still persists and here its height can be controlled in general by the chiral symmetry breaking field  $m$  as also  $\text{Im} \Gamma_{ad}^i$ . As shown in Fig. 7a-b), the electronic spin polarisation of the MF wavefunctions are also in this case confined to the  $x-z$  plane. *In addition, both wavefunctions are real or imaginary.* Therefore, by employing a tip with polarisation along the  $y$  axis one simultaneously induces finite values for  $m$  and  $\text{Im} \Gamma_{ad}^i$ . For a spin-polarisation of the tip in the  $x-z$  plane or an unpolarised tip,  $m = \text{Im} \Gamma_{ad}^i = 0$ . Therefore, in the latter cases we obtain a ZBP with double unit of conductance [10], as if the 2 MFs were unpaired [4].

When chiral symmetry is preserved ( $m = \text{Im} \Gamma_{ad}^i = 0$ ), one obtains the following profile for a general voltage bias

$$\frac{dI_i}{dV} = \frac{2e^2}{h} \cdot \frac{2 \det^2(\hat{\Gamma}^i) + (eV)^2 \left[ (\Gamma_{aa}^i)^2 + (\Gamma_{ee}^i)^2 + 2(\Gamma_{ae}^i)^2 \right]}{\left[ (eV)^2 - \det \hat{\Gamma}^i \right]^2 + (eV)^2 (\Gamma_{aa}^i + \Gamma_{ee}^i)^2}, \quad (47)$$

One observes that only the first summand is responsible for the double unit of conductance ZBP, while the second term of the above equation contributes beyond a crossover voltage where the sharp spike profile switches to a broad hump feature. Essentially, for very small voltages the two MFs behave as unpaired and beyond the crossover voltage they couple giving rise to two FBPs. This is obvious from the contribution of the second summand depicted with the orange line in Fig. 7b).

Note finally that there also special cases in which the presence of 2 MFs per edge can be even *masked* and

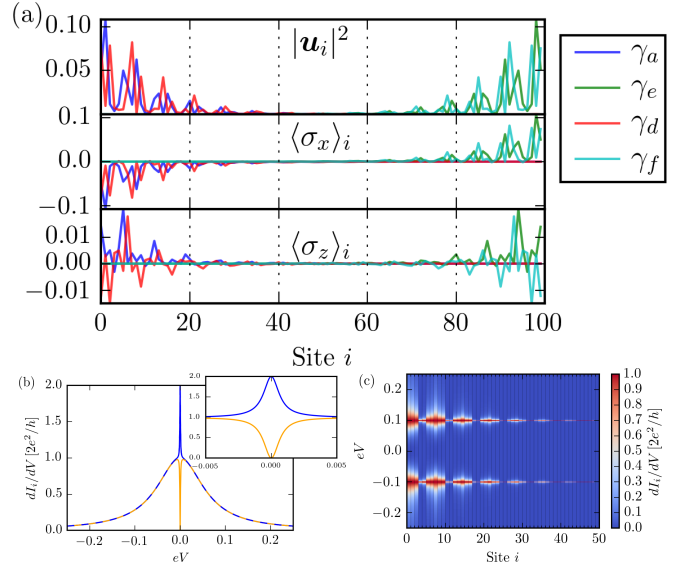


FIG. 7. (a) MF spectral weight  $|u_i|^2$  and electronic spin-polarisation. The spin-polarisation has only  $x, z$  components. (b) Profile of the double unit of conductance ZBP when chiral symmetry is preserved. There exists a crossover voltage at which the spike-like profile switches to a broad hump-feature. This reflects the contribution of two different sources to the conductance. The blue curve shows the full conductance, whereas the orange curve shows only the contribution of the second summand in Eq. (48). In the inset we zoom around  $V = 0$ . (c) Spatial tunneling conductance profile for broken chiral symmetry ( $m = 0.1$ ) and spin unpolarised tip. Parameters:  $N = 100$ ,  $\xi_0 = 80$ ,  $k_F = 6.0$ ,  $\alpha = 0.01$  and  $M = 0.85$ .

misinterpreted as a single MF per edge. In fact, if chiral symmetry is preserved and for some particular values the condition  $\Gamma_{aa}^i \Gamma_{dd}^i = (\Gamma_{ad}^i)^2 = \text{Re}^2 \Gamma_{ad}^i$  additionally holds, then we obtain the expression for the tunneling conductance

$$\frac{dI_i}{dV} = \frac{2e^2}{h} \frac{(\Gamma_{aa}^i + \Gamma_{dd}^i)^2}{(eV)^2 + (\Gamma_{aa}^i + \Gamma_{dd}^i)^2}, \quad (48)$$

which is identical to the one for a single MF per edge but with an effective broadening  $\Gamma_{aa}^i + \Gamma_{dd}^i$ . The special condition satisfied above implies that essentially only one MF of the chiral symmetry protected MF pair is seen by the SPSTM tip.

### C. Two TSC chains with 1 MF per edge

We now consider two coupled chains, each of which can harbor a single MF per edge, a situation depicted in Fig. 8. The particular setup can be useful for indirectly probing the  $4\pi$ -periodic Josephson effect. By assuming that the two chains are sufficiently long so that the MFs away from the junction can be excluded from our analy-



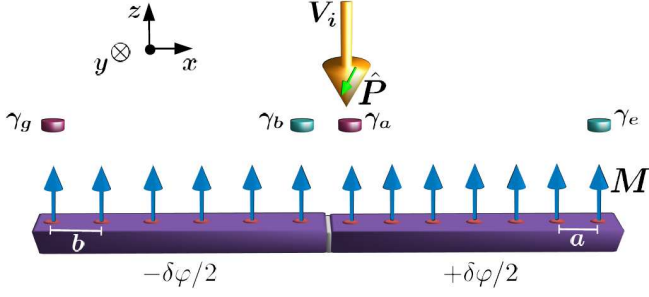


FIG. 8. Josephson junction of two tunnel-coupled TSC chains each of which harbors 1 MF per edge. For sufficiently long chains only the two MFs near the junction need to be taken into account. Here only  $\gamma_a$  couples to the SPSTM tip. The coupling  $M$  of  $\gamma_a$  and  $\gamma_b$  has form of  $4\pi$ -periodic Josephson term.

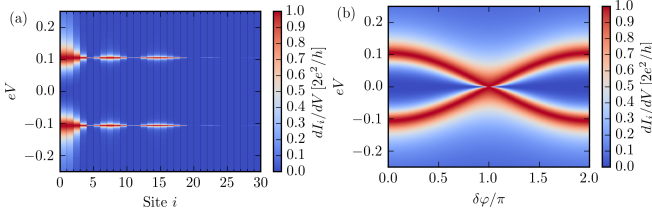


FIG. 9. (a) Spatial profile of the tunneling conductance for  $\delta\varphi = 0$ . One obtain two FFBs at  $eV = \pm M(\delta\varphi)$  (b)  $2\pi$ -periodic dependence of the tunneling conductance on the superconducting phase difference  $\delta\varphi$ . For  $\delta\varphi = \pi$  one recovers the ZBP. We used a tunneling constant  $t = 0.1$  and a decay length  $l = 10$ .

sis, we obtain

$$\widehat{\mathcal{M}} = \begin{pmatrix} 0 & M \\ -M & 0 \end{pmatrix} \quad \text{and} \quad \widehat{\Gamma}^i = \begin{pmatrix} \Gamma_{aa}^i & 0 \\ 0 & 0 \end{pmatrix}. \quad (49)$$

In this case the MF coupling matrix element originates from interchain tunneling and has the form

$$M = 4 \text{Im} \sum_{i,j,\sigma} u_{i,\sigma,a}^* T_{i,j} e^{i(\varphi_i - \varphi_j)/2} u_{j,\sigma,b}. \quad (50)$$

Similarly to Eq. (44) one obtains for the particular case

$$\frac{dI_i}{dV} = \frac{2e^2}{h} \frac{(eV)^2 (\Gamma_{aa}^i)^2}{[(eV)^2 - M^2]^2 + (eV)^2 (\Gamma_{aa}^i)^2}. \quad (51)$$

Therefore, by imposing a difference  $\delta\varphi$  between the phases of the two SCs, we can tune  $M$  and modify the FFBs. The tunneling conductance is a  $2\pi$ -periodic function of  $\delta\varphi$ , resulting from the  $4\pi$ -periodic Josephson coupling  $\propto \cos(\delta\varphi/2)$  between the  $\gamma_a$  and  $\gamma_b$ .

#### D. Two coupled TSC chains: one with 1 MF per edge (below the tip) and one with 2 MFs per edge

As previously we concentrate on the MFs near the junction. In this case only  $\gamma_a$  couples to the tip and

we have

$$\widehat{\mathcal{M}} = \begin{pmatrix} 0 & M_{ab} & M_{ac} \\ -M_{ab} & 0 & m_{bc} \\ -M_{ac} & -m_{bc} & 0 \end{pmatrix}, \quad \widehat{\Gamma}^i = \begin{pmatrix} \Gamma_{aa}^i & 0 & 0 \\ 0 & 0 & 0 \\ 0 & 0 & 0 \end{pmatrix}. \quad (52)$$

The matrix elements  $M_{ab}$  and  $M_{ac}$  originate from interchain tunneling while  $m_{bc}$  originates from chiral symmetry breaking only in the left or even in both chains. Weak violation of chiral symmetry does not introduce any modification to the wavefunction of the  $\gamma_a$  MF. Thus in the particular case, we obtain the conductance formula

$$\frac{dI_i}{dV} = \frac{2e^2}{h} \frac{[(eV)^2 - m_{bc}^2]^2 (\Gamma_{aa}^i)^2}{(eV)^2 [(eV)^2 - \mathcal{M}^2]^2 + (\Gamma_{aa}^i)^2 [(eV)^2 - m_{bc}^2]^2}, \quad (53)$$

with  $\mathcal{M} = \sqrt{M_{ab}^2 + M_{ac}^2 + m_{bc}^2}$ . For  $V = 0$  we observe that we obtain the ZBP. Indeed, this confirms the rule derived in Ref. 10 according to which the tunneling conductance of an odd number of coupled MFs demonstrate the ZBP. Moreover there are also two FFBs of  $2e^2/h$  at  $eV = \pm \mathcal{M}$ . However, if chiral symmetry is preserved, i.e.  $m_{bc} = 0$ , we obtain

$$\frac{dI_i}{dV} = \frac{2e^2}{h} \frac{(eV)^2 (\Gamma_{aa}^i)^2}{[(eV)^2 - M^2]^2 + (eV)^2 (\Gamma_{aa}^i)^2}. \quad (54)$$

Essentially if chiral symmetry is preserved the system behaves as only 2 MFs become coupled, with an effective coupling  $M = \sqrt{M_{ab}^2 + M_{ac}^2}$ . This becomes transparent by writing  $i\gamma_a(M_{ab}\gamma_b + M_{ac}\gamma_c) = iM\gamma_a(M_{ab}\gamma_b/M + M_{ac}\gamma_c/M)$ . The orthogonal linear combination of MFs  $M_{ac}\gamma_b - M_{ab}\gamma_c$  remains unpaired [4] and unseen by the SPSTM tip. Therefore switching on and off the chiral symmetry breaking field can controllably make the ZBP appear or disappear providing a smoking gun signature of MFs in these chains. On the other hand, one by controlling  $\delta\varphi$  can shift the two split peaks at  $eV = \pm M$ , adding another experimental knob for detecting MFs.

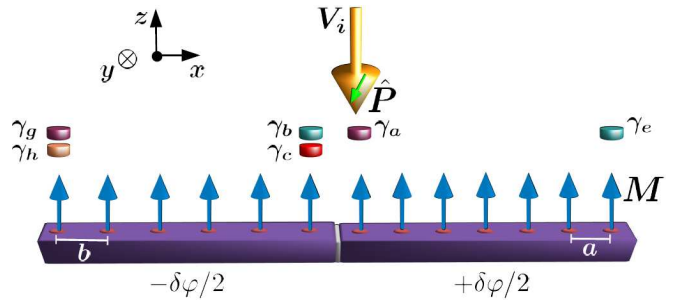


FIG. 10. Josephson junction of two tunnel-coupled TSC chains harboring a different MF number per edge (two and one respectively). For sufficiently long chains, only the three MFs near the junction need to be taken into account. Here only  $\gamma_a$  couples to the SPSTM tip. The couplings  $M$  of  $\gamma_a$  to  $\gamma_b$  and  $\gamma_c$  have the form of  $4\pi$ -periodic Josephson terms. Chiral symmetry breaking can further mix  $\gamma_b$  and  $\gamma_c$ .

### E. Two coupled TSC chains: one with 1 MF per edge and one with 2 MFs per edge (below the tip)

In the present paragraph we consider the second possible configuration for two chains with uneven edge MF number, as shown in the Fig. 11. In the particular case one obtains the matrices

$$\widehat{\mathcal{M}} = \begin{pmatrix} 0 & m_{ad} & M_{ab} \\ -m_{ad} & 0 & M_{db} \\ -M_{ab} & -M_{db} & 0 \end{pmatrix}, \widehat{\Gamma}^i = \begin{pmatrix} \Gamma_{aa}^i & \Gamma_{ad}^i & 0 \\ (\Gamma_{ad}^i)^* & \Gamma_{dd}^i & 0 \\ 0 & 0 & 0 \end{pmatrix}. \quad (55)$$

The matrix elements  $M_{ab}$  and  $M_{db}$  originate from inter-chain tunneling while  $m_{ad}$  originates from chiral symmetry breaking in the particular or even both chains. Weakly breaking chiral symmetry does not affect the wavefunction of the single edge MF.

Here the resulting tunneling conductance expression is lengthy and therefore we present it in the Appendix. However, one can directly infer that the ZBP persists *both* in the presence or absence of chiral symmetry. The reason is that the MFs below the tip become always indirectly coupled via their interaction with the tip, and thus the presence or not of chiral symmetry is only important for ensuring the presence of the 2 MFs. Since all three MFs are coupled and their number is odd the appearance of the ZBP was expected according to the rule of Ref. 10. If the couplings to  $\gamma_b$  become zero, then we return to the case of 2 MFs at the edge of a single chain discussed in Sec. III B, in which case the existence of a ZBP crucially depends on the persistence of chiral symmetry.

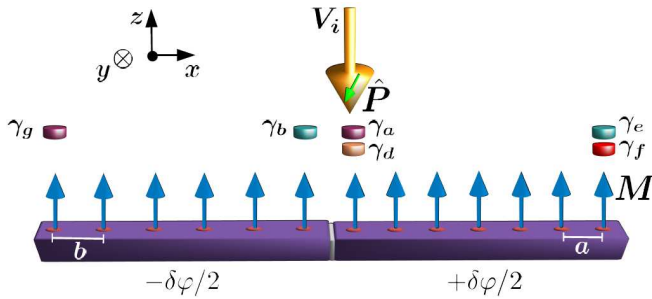


FIG. 11. Josephson junction of two tunnel-coupled TSC chains harboring a different MF number per edge (one and two respectively). For sufficiently long chains, only the three MFs near the junction need to be taken into account. Here only the chiral symmetry protected MF pair  $\gamma_a$  and  $\gamma_d$  couple to the SPSTM tip. The couplings  $M$  of  $\gamma_b$  to  $\gamma_a$  and  $\gamma_d$  have the form of  $4\pi$ -periodic Josephson terms. If chiral symmetry is broken  $\gamma_a$  and  $\gamma_d$  can also have a finite coupling.

### F. Two TSC chains: Both with 2 MFs per edge

For completing our analysis we proceed with examining the case in which both chains harbor 2 MFs per edge and are tunnel-coupled. By focusing only on the MFs near the junction depicted in Fig. 1 we can write

$$\widehat{\mathcal{M}} = \begin{pmatrix} 0 & m_{ad} & M_{ac} & M_{ab} \\ -m_{ad} & 0 & M_{dc} & M_{db} \\ -M_{ac} & -M_{dc} & 0 & m_{cb} \\ -M_{ab} & -M_{db} & -m_{cb} & 0 \end{pmatrix}, \quad (56)$$

$$\widehat{\Gamma}^i = \begin{pmatrix} \Gamma_{aa}^i & \Gamma_{ad}^i & 0 & 0 \\ (\Gamma_{ad}^i)^* & \Gamma_{dd}^i & 0 & 0 \\ 0 & 0 & 0 & 0 \\ 0 & 0 & 0 & 0 \end{pmatrix}, \widehat{M} = \begin{pmatrix} M_{ac} & M_{ab} \\ M_{dc} & M_{db} \end{pmatrix}. \quad (57)$$

The expression that one obtains for the tunneling conductance is lengthy and therefore we do not include it in this manuscript. However it is easy to retain the expression for the tunneling conductance at  $V = 0$ , which is sufficient for providing information about the qualitative characteristics of the system. The zero voltage conductance reads

$$\left. \frac{dI_i}{dV} \right|_{V=0} = \frac{2e^2}{h} \frac{2m_{cb}^2 \det \widehat{\Gamma}^i}{\left( \det \widehat{M} - m_{ad} m_{cb} \right)^2 + m_{cb}^2 \det(\text{Re} \widehat{\Gamma}^i)}. \quad (58)$$

It is straightforward to observe that we obtain a ZBP but the conductance does not take a quantised value. At this point we can further focus on special cases. If chiral symmetry is at least restored for the chain which does not couple to the SPSTM tip (i.e.  $m_{cb} = 0$ ), the ZBP vanishes, implying that effectively an even number of MFs out of the four are essentially probed by the tip. On the other hand, if chiral symmetry is only restored for the chain probed by the tip (i.e.  $m_{ad} = 0$  and  $P_y = 0$ ), the ZBP remains but with modified and still non-quantised conductance value. Note however that if  $m_{ad} = 0$  and  $\det \widehat{M} = 0$  then we obtain a peak of a double unit of conductance as if only two unpaired MFs appear in the system. Finally, if only  $\det \widehat{M} = 0$ , the tunnel coupling matrix has a zero eigenvalue implying that the tip does not see the second chain and we return to the case of 2 MFs probed simultaneously by the tip.

## IV. CONCLUSIONS

We explored new distinctive MF features which can be measured via spin-polarised scanning tunneling microscopy in hybrid devices consisting of ferromagnetic chains on top of spin-orbit coupled superconductors. For the calculations we adopted a microscopic model describing Yu-Shiba-Rusinov chains which can harbor 1 or 2 MFs per edge if chiral symmetry is present. For an isolated topological YSR chain with a single MF per

edge, we showed that the tunneling conductance delicately depends on the direction along which the tip is spin-polarised. In fact, for a fully spin-polarised tip there can be special angles of the tip polarisation for which the conductance vanishes. In addition, in the case of short chains where MFs on both edges contribute, one finds that depending on the tip polarisation the signal can be extremely weak while at the same time other directions support an almost quantised ZBP. This can be relevant for the recent measurements of Ref. 2 which were characterised by a weak signal. According to our findings, the polarisation and Zeeman field of the experiment (i.e.  $z$  axis) were oriented along the direction for which the MF signal appears to be the lowest. Altering the field angle would naturally lead to signal enhancement and allow the possible observation of the long-sought-for ZBP. Moreover, we showed that in the case of a single chain with 2 symmetry protected MFs per edge, the tip (or an additional Zeeman field along the  $y$  axis) can induce a weak symmetry violating term which can controllably

modify the tunneling spectra. In addition, for the case of tunnel-coupled topological chains, one can induce a difference between the phases of the two superconductors in order to modify the location of emerging finite bias peaks via the  $4\pi$ -Josephson coupling. In fact, the tunneling conductance could be used as an indirect probe of the latter. Furthermore, for two chains with different edge MF number, tunable chiral symmetry violation and restoration can switch on and off the ZBP which is a robust MF feature. This new set of MF characteristics relying on the MF spin-polarisation, which were extracted from a realistic YSR microscopic model for these chains, reveals new experimental methods for unambiguously detecting MFs in the near future.

## ACKNOWLEDGMENTS

PK is grateful to A. Shnirman and S. Kourtis for fruitful and insightful discussions.

- 
- [1] V. Mourik, K. Zuo, S. M. Frolov, S. R. Plissard, E. P. A. M. Bakkers, and L. P. Kouwenhoven, *Science* **336**, 1003 (2012); M. T. Deng, C. L. Yu, G. Y. Huang, M. Larsson, P. Caroff, and H. Q. Xu, *Nano Lett.* **12**, 6414 (2012); L. P. Rokhinson, Xinyu Liu, and J. K. Furdyna, *Nano Lett.* **8**, 795 (2012); A. Das, Y. Ronen, Y. Most, Y. Oreg, M. Heiblum, and H. Shtrikman, *Nano Lett.* **8**, 887 (2012).
  - [2] S. Nadj-Perge, I. K. Drozdov, J. Li, H. Chen, S. Jeon, J. Seo, A. H. MacDonald, B. A. Bernevig, and A. Yazdani, *Science* **346**, 602 (2014).
  - [3] R. Pawlak, M. Kisiel, J. Klinovaja, T. Meier, S. Kawai, T. Glatzel, D. Loss, and E. Meyer, *arXiv:1505.06078* (2015).
  - [4] A. Yu. Kitaev, *Phys.-Usp.* **44**, 131 (2001).
  - [5] L. Fu and C. L. Kane, *Phys. Rev. Lett.* **100**, 096407 (2008); J. Alicea, *Rep. Prog. Phys.* **75**, 076501 (2012); C. W. J. Beenakker, *Annu. Rev. Con. Mat. Phys.* **4**, 113 (2013).
  - [6] P. Kotetes, *New J. Phys.* **15**, 105027 (2013).
  - [7] A. Yu. Kitaev, *Annals Phys.* **303**, 2 (2003); C. Nayak, S. H. Simon, A. Stern, M. Freedman, and S. Das Sarma, *Rev. Mod. Phys.* **80**, 1083 (2008); N. Read and D. Green, *Phys. Rev. B* **61**, 10267 (2000); D. A. Ivanov, *Phys. Rev. Lett.* **86**, 268 (2001); J. Alicea, Y. Oreg, G. Refael, F. von Oppen, and M. P. A. Fisher, *Nat. Physics* **7**, 412 (2011).
  - [8] R. M. Lutchyn, J. D. Sau and S. Das Sarma, *Phys. Rev. Lett.* **105**, 077001 (2010); Y. Oreg, G. Refael and F. von Oppen, *Phys. Rev. Lett.* **105**, 177002 (2010).
  - [9] K. T. Law, Patrick A. Lee, and T. K. Ng, *Phys. Rev. Lett.* **103**, 237001 (2009).
  - [10] K. Flensberg, *Phys. Rev. B* **82**, 180516(R) (2010).
  - [11] J. Liu, A. C. Potter, K. T. Law, and P. A. Lee, *Phys. Rev. Lett.* **109**, 267002 (2012); D. I. Pikulin, J. P. Dahlhaus, M. Wimmer, H. Schomerus, and C. W. J. Beenakker, *New J. Phys.* **14**, 125011 (2012); G. Kells, D. Meidan, and P. W. Brouwer, *Phys. Rev. B* **86**, 100503 (2012).
  - [12] E. J. H. Lee, X. Jiang, R. Aguado, G. Katsaros, C. M. Lieber, and S. De Franceschi, *Phys. Rev. Lett.* **109**, 186802 (2012); E. J. H. Lee, X. Jiang, M. Houzet, R. Aguado, C. M. Lieber, and S. De Franceschi, *Nat. Nanotechnol.* **9**, 79 (2014); A. D. K. Finck, D. J. Van Harlingen, P. K. Mohseni, K. Jung, and X. Li, *Phys. Rev. Lett.* **110**, 126406 (2013); H. O. H. Churchill, V. Fatemi, K. Grove-Rasmussen, M. T. Deng, P. Caroff, H. Q. Xu, and C. M. Marcus, *Phys. Rev. B* **87**, 241401(R) (2013).
  - [13] T.-P. Choy, J. M. Edge, A. R. Akhmerov, and C. W. J. Beenakker, *Phys. Rev. B* **84**, 195442 (2011).
  - [14] I. Martin and A. F. Morpurgo, *Phys. Rev. B* **85**, 144505 (2012).
  - [15] M. Kjaergaard, K. Wölms and K. Flensberg, *Phys. Rev. B* **85**, 020503 (2012).
  - [16] S. Nadj-Perge, I. K. Drozdov, B. A. Bernevig, and A. Yazdani, *Phys. Rev. B* **88**, 020407(R) (2013).
  - [17] S. Nakosai, Y. Tanaka, and N. Nagaosa, *Phys. Rev. B* **88**, 180503(R) (2013); B. Braunecker and P. Simon, *Phys. Rev. Lett.* **111**, 147202 (2013); J. Klinovaja, P. Stano, A. Yazdani, and D. Loss, *Phys. Rev. Lett.* **111**, 186805 (2013); M. M. Vazifeh and M. Franz, *Phys. Rev. Lett.* **111**, 206802 (2013); F. Pientka, L.I. Glazman, F. von Oppen, *Phys. Rev. B* **88**, 155420 (2013); *Phys. Rev. B* **89**, 180505(R) (2014); K. Pöyhönen, A. Westström, J. Röntynen, T. Ojanen, *Phys. Rev. B* **89**, 115109 (2014); J. Röntynen and T. Ojanen, *Phys. Rev. B* **90**, 180503 (2014); Y. Kim, M. Cheng, B. Bauer, R. M. Lutchyn, S. Das Sarma, *Phys. Rev. B* **90**, 060401(R) (2014); N. Sedlmayr, J. M. Aguiar-Hualde, and C. Bena, *Phys. Rev. B* **91**, 115415 (2015).
  - [18] A. Heimes, P. Kotetes, and G. Schön, *Phys. Rev. B* **90**, 060507 (2014).
  - [19] P. M. R. Brydon, H.-Y. Hui, and J. D. Sau, *Phys. Rev. B* **91**, 064505 (2015).
  - [20] Jian Li, Hua Chen, I. K. Drozdov, A. Yazdani, B. A. Bernevig, and A. H. MacDonald, *Phys. Rev. B* **90**, 235433 (2014).

- [21] A. Heimes, D. Mendler, and P. Kotetes, New J. Phys. **17** 023051 (2015).  
 [22] H. Ebisu, K. Yada, H. Kasai, and Y. Tanaka, Phys. Rev. B **91**, 054518 (2015).  
 [23] Y. Peng, F. Pientka, L. I. Glazman, and F. von Oppen, Phys. Rev. Lett. **114**, 106801 (2015).  
 [24] J. Zhang, Y. Kim, E. Rossi, and R. M. Lutchyn, arXiv:1505.05862 (2015).  
 [25] S. Das Sarma, Hoi-Yin Hui, P. M. R. Brydon, and Jay D. Sau, arXiv:1503.00594 (2015).  
 [26] T. Cadez and P. D. Sacramento, arXiv:1506.07909 (2015).  
 [27] Y. Peng, F. Pientka, Y. Vinkler-Aviv, L. I. Glazman, F. von Oppen, arXiv:1506.06763 (2015).  
 [28] L. Yu, Acta Phys. Sin. **21**, 75 (1965).  
 [29] H. Shiba, Prog. Theor. Phys. **40**, 435 (1968).  
 [30] A. I. Rusinov, Sov. Phys. JETP **29**, 1101 (1969).  
 [31] A. Yazdani, B. A. Jones, C. P. Lutz, M. F. Crommie, and D. M. Eigler, Science **275**, 1767 (1997).  
 [32] L. Fu and C. L. Kane, Phys. Rev. B **79**, 161408(R) (2009); P. Kotetes, G. Schön, and A. Shnirman, J. Korean Phys. Soc. **62**, 1558 (2013); L. Jiang, D. Pekker, J. Alicea, G. Refael, Y. Oreg, A. Brataas, and F. von Oppen, Phys. Rev. B **87**, 075438 (2013).  
 [33] A. Altland and M. R. Zirnbauer, Phys. Rev. B **55**, 1142 (1997); A. Kitaev AIP Conf. Proc., **1134**, 22 (2009); S. Ryu, A. Schnyder, A. Furusaki and A. Ludwig, New J. Phys. **12** 065010 (2010); M. Koshino, T. Morimoto, and M. Sato, Phys. Rev. B **90**, 115207 (2014).  
 [34] H.-Y. Hui, P. M. R. Brydon, J. D. Sau, S. Tewari, and S. Das Sarma, Sci. Rep. **5**, 8880 (2015).  
 [35] J. Röntynen and T. Ojanen, Phys. Rev. Lett. **114**, 236803 (2015).

### Appendix: Expression for the tunneling conductance for the case presented in Sec. III E

$$\frac{dI_i}{dV} = \frac{2e^2}{h} \frac{N(eV)}{D(eV)}, \quad (\text{A.1})$$

where we have introduced the denominator

$$\begin{aligned} D(\omega) = & \omega^6 + \omega^4 [(\Gamma_{aa}^i)^2 + (\Gamma_{dd}^i)^2 + 2\text{Re}^2 \Gamma_{ad}^i - 2\mathcal{M}^2] \\ & + \omega^2 \left\{ [\Gamma_{aa}^i \Gamma_{dd}^i - \text{Re}^2 \Gamma_{ad}^i + \mathcal{M}^2]^2 - 2(\Gamma_{aa}^i + \Gamma_{dd}^i) [\Gamma_{aa}^i M_{db}^2 + \Gamma_{dd}^i M_{ab}^2 - 2(\text{Re} \Gamma_{ad}^i) M_{ab} M_{db}] \right\} \\ & + [\Gamma_{aa}^i M_{db}^2 + \Gamma_{dd}^i M_{ab}^2 - 2(\text{Re} \Gamma_{ad}^i) M_{ab} M_{db}]^2, \end{aligned} \quad (\text{A.2})$$

and the nominator

$$\begin{aligned} N(\omega) = & \omega^4 \{ (\Gamma_{aa}^i)^2 + (\Gamma_{dd}^i)^2 + 2[\text{Re}^2 \Gamma_{ad}^i - \text{Im}^2 \Gamma_{ad}^i] \} + 2\omega^2 [\Gamma_{aa}^i \Gamma_{dd}^i - \text{Re}^2 \Gamma_{ad}^i + m_{ad}^2] [\Gamma_{aa}^i \Gamma_{dd}^i - |\Gamma_{ad}^i|^2] \\ & - 2\omega^2 \{ [(\Gamma_{aa}^i)^2 + \text{Re}^2 \Gamma_{ad}^i - \text{Im}^2 \Gamma_{ad}^i] M_{db}^2 + [(\Gamma_{dd}^i)^2 + \text{Re}^2 \Gamma_{ad}^i - \text{Im}^2 \Gamma_{ad}^i] M_{ab}^2 - 2(\Gamma_{aa}^i + \Gamma_{dd}^i)(\text{Re} \Gamma_{ad}^i) M_{ab} M_{db} \} \\ & + [\Gamma_{aa}^i M_{db}^2 + \Gamma_{dd}^i M_{ab}^2 - 2(\text{Re} \Gamma_{ad}^i) M_{ab} M_{db}]^2, \end{aligned} \quad (\text{A.3})$$

with  $\mathcal{M} = \sqrt{m_{ad}^2 + M_{ab}^2 + M_{db}^2}$ .